

Depletion of intermediate filament protein Nestin, a target of microRNA-940, suppresses tumorigenesis by inducing spontaneous DNA damage accumulation in human nasopharyngeal carcinoma

J Ma^{1,2,6}, F Sun^{*,3,6}, C Li^{4,6}, Y Zhang², W Xiao², Z Li⁴, Q Pan², H Zeng⁵, G Xiao⁴, K Yao⁴, A Hong^{*,1} and J An^{*,4}

Nasopharyngeal carcinoma (NPC) is a major malignant tumor of the head and neck region in southern China. The understanding of its underlying etiology is essential for the development of novel effective therapies. We report for the first time that microRNA-940 (miR-940) significantly suppresses the proliferation of a variety of cancer cell lines, arrests cells cycle, induces caspase-3/7-dependent apoptosis and inhibits the formation of NPC xenograft tumors in mice. We further show that miR-940 directly binds to the 3'-untranslated regions of Nestin mRNA and promotes its degradation. Likewise, depletion of Nestin inhibits tumor cell proliferation, arrest cells at G2/M, induces apoptosis and suppresses xenograft tumor formation *in vivo*. These functions of miR-940 can be reversed by ectopic expression of Nestin, suggesting that miR-940 regulates cell proliferation and survival through Nestin. Notably, we observed reduced miR-940 and increased Nestin levels in NPC patient samples. Protein microarray revealed that knockdown of Nestin in 5-8F NPC cells alters the phosphorylation of proteins involved in the DNA damage response, suggesting a mechanism for the miR-940/Nestin axis. Consistently, depletion of Nestin induced spontaneous DNA damage accumulation, delayed the DNA damage repair process and increased the sensitivity to irradiation and the chemotherapeutic agent doxorubicin. Collectively, our findings indicate that Nestin, which is downregulated by miR-940, can promote tumorigenesis in NPC cells through involvement in the DNA damage response. The levels of microRNA-940 and Nestin may serve as indicators of cancer status and prognosis.

Cell Death and Disease (2014) 5, e1377; doi:10.1038/cddis.2014.293; published online 14 August 2014

Nasopharyngeal carcinoma (NPC), a major malignant tumor of the head and neck region, is endemic to Southeast Asia, southern China, the Arctic, the Middle East and North Africa.¹ Low differentiation and high metastatic potential and recurrence rates are major pathologic features of NPC. The incidence of NPC in southern China has remained very high, with a 5-year overall survival rate of approximately 70%.² Within 4 years after radiation therapy, about 30–40% of NPC patients develop distant metastasis, which is associated with poor prognosis.³ Therefore, an understanding of the underlying etiology is essential for the development of novel effective therapies for NPC.

MicroRNAs (miRNAs), a class of small (~22 nucleotides) noncoding RNAs, reduce mRNA stability and/or suppress

translation by binding to the 3'-untranslated regions (3'-UTRs) or coding sequences of target mRNAs.⁴ As such, miRNAs are involved in the majority of basic biologic processes, including cell proliferation, apoptosis, differentiation and development.⁵ Cumulative evidence also suggests that miRNAs can function as potential oncogenes or tumor suppressor genes.^{6,7} Abnormal expression of miRNAs and mutations of their genes have been documented in various types of tumors.⁸ Recently, a growing number of miRNAs have been implicated in the development of NPC. For instance, the decreased expression of miR-100 has been reported to cause Plk1 overexpression, which in turn contributes to NPC progression.⁹ MiR-200a upregulation in the undifferentiated cell line C666-1 inhibits cell growth, migration and invasion by targeting ZEB2 and

¹Institute of Genetic Engineering, Jinan University, National Engineering Research Center of Genetic Medicine, Key Lab for Genetic Medicine of Guangdong Province, Guangzhou, People's Republic of China; ²Central Laboratory, Shanghai 10th People's Hospital of Tongji University, Shanghai, People's Republic of China; ³Department of Medical Laboratory, Shanghai 10th People's Hospital of Tongji University, Shanghai, People's Republic of China; ⁴Cancer Research Institute, Southern Medical University, Guangzhou, People's Republic of China and ⁵Department of Pathology, Sun Yat-sen Memorial Hospital, Sun Yat-sen University, Guangzhou, People's Republic of China

*Corresponding author: F Sun, Department of Medical Laboratory, Shanghai 10th People's Hospital of Tongji University, Shanghai 200072, People's Republic of China. Tel/Fax: +86 21 66306909; E-mail: sunfenyong2012@gmail.com

or A Hong, Institute of Genetic Engineering, Jinan University, National Engineering Research Center of Genetic Medicine, Key Lab for Genetic Medicine of Guangdong Province, Guangzhou, 510632, People's Republic of China. Tel: +86 20 85223266; Fax: +86 20 85221983; E-mail: tha@jnu.edu.cn

or J An, Cancer Research Institute, Southern Medical University, Guangzhou 510515, People's Republic of China. Tel/Fax: +86 20 61648709; E-mail: anjing77@gmail.com

⁶These authors contributed equally to this work.

Abbreviations: NPC, nasopharyngeal carcinoma; DDR, DNA damage response; IR, ionizing radiation; miRNAs, microRNAs; miR-940, microRNA-940; 3'-UTRs, 3'-untranslated regions; PI, propidium iodide; FACS, fluorescence-activated cell sorting; NES, Nestin; Dox, doxorubicin; DSBs, DNA double-strand breaks; Cdk5, cyclin-dependent kinase 5

Received 10.2.14; revised 26.5.14; accepted 09.6.14; Edited by G Calin

CTNNB1.¹⁰ Inhibition of miR-141, which is upregulated in NPC specimens, may affect cell cycle, apoptosis, cell growth, migration and invasion through targeting of BRD3, UBAP1 and PTEN.¹¹ In addition, reduced levels of let-7 in NPC might have a role in the proliferation through DNA methylation.¹² In view of the roles of miRNAs in tumorigenesis, identification of key miRNAs and their targets that contribute to NPC progression may provide novel targets for NPC diagnosis and treatment.

Nestin, a member of the type VI intermediate filament protein family, is widely expressed in mammalian nervous tissue, some immortalized mammalian stem cell lines¹³ and precursor cells of some tissues, for which expression is decreased with differentiation.^{14–16} As a stem cell/progenitor cell marker,¹⁷ Nestin is essential for mitogen-stimulated proliferation of neural progenitor cells,¹⁸ and loss of Nestin leads to apoptosis of neural progenitor cells in zebrafish.¹⁹ Recently, Nestin has been detected in various cell lines established from human solid tumors²⁰ and has been associated with aggressive nervous system tumors.²¹ All of these findings suggest that Nestin is associated with tumorigenesis; however, the precise role of Nestin and the relationship between Nestin and NPC progression are still unknown.

In this study, we screen 350 different miRNAs and determined that miR-940 inhibits the proliferation of the NPC cell lines 5-8F and CNE2. Furthermore, miR-940 expression induces G2/M arrest, promotes apoptosis and suppresses xenograft tumor growth. Bioinformatic and luciferase reporter assays revealed that miR-940 targets two putative binding sites in the Nestin 3'-UTR region. A physiologic role for miR-940 was suggested by its common downregulation in NPC tissues, whereas Nestin showed a converse pattern of upregulation. Knockdown of Nestin in 5-8F and CNE2 cells induces G2/M arrest and apoptosis and inhibits cell proliferation and xenograft tumor growth; conversely, ectopic expression of Nestin partially reverses the effects of miR-940 on cell proliferation, cell cycle and apoptosis. Interestingly, knockdown of Nestin induces spontaneous DNA damage accumulation, delays DNA damage repair and enhances sensitivity to ionizing radiation (IR) of 5-8F cells both *in vitro* and *in vivo*. These results elucidate a pathway by which miR-940 regulates tumor progression in NPC by targeting Nestin.

Results

MiR-940 exhibits tumor suppression function. To screen for miRNAs that can promote or inhibit NPC cell proliferation, we transfected 350 different miRNAs into 5-8F individually and then measured cell growth by MTT assay. Four miRNAs (miR-21, miR-221, miR-222 and miR-650) significantly promoted cell proliferation, whereas seven miRNAs (miR-143, miR-200a, miR-200c, miR-29c, miR-34a, miR-375 and miR-940) suppressed cell proliferation. Because miR-940 has not been well studied, we focused on the potential role of miR-940 in suppressing NPC cell growth. We transfected miR-940 precursor into NPC cell lines 5-8F and CNE2 to increase the levels of ectopic miR-940 (Supplementary Figure 1A), and determined that miR-940 elevation not only inhibited cell proliferation (Figures 1a and b) but also led to G2/M cell cycle arrest (Supplementary Figure 2A).

Furthermore, fluorescence-activated cell sorting (FACS) analysis indicated that overexpression of miR-940 induced cell apoptosis (Supplementary Figure 2B), which is mediated by caspase-3/7 activation (Figure 1c). We verified the effect of miR-940 on cell proliferation in eight additional cancer cell lines, including the NPC cell lines 6-10B and CNE-1; the esophageal cancer cell lines EC-1, EC-9706, KYSE-150 and TE-1; and the liver cancer cell lines MHCC97-H and QGY-7701 (Supplementary Figures 3A–C).

To assess the *in vivo* effect of ectopic miR-940 expression, 5-8F cells infected with miR-940-expressing lentivirus were subcutaneously inoculated into nude mice. The tumors formed in the presence of miR-940-overexpressing xenografts were much smaller than those of the control cells (Figures 1d–f). Furthermore, consistent with a physiologic role for miR-940 in suppressing NPC, the levels of miR-940 were 1.84-fold lower in NPC patient samples compared with their corresponding adjacent normal tissues ($P = 1.50E - 05$) (Figure 1g). These data suggest that miR-940 is a novel tumor suppressor miRNA, which exerts its function by inhibiting tumor cell proliferation and promoting apoptosis.

Mir-940 regulates Nestin in nasopharyngeal cancer. To explore the molecular mechanism by which miR-940 regulates cell proliferation and apoptosis, we performed microarray expression profiling using 5-8F cells transfected with miR-940 precursor for 0, 12, 24 and 48 h. Unsupervised hierarchical clustering analysis is shown in Supplementary Figure 4A. By gene ontology, differentially expressed genes can be divided into three groups of similar biologic processes: regulation of apoptosis, cell cycle and cell proliferation (Supplementary Figures 4B–D and Supplementary Table 1). To further predict the putative targets of miR-940, we performed bioinformatic analysis. Among 48 000 genes in the Microarray database (Figure 2a, section I), 359 genes were predicted as possible targets of miR-940 in fRNAdb, a database for annotating noncoding transcripts acquired from publicly available databases (section II). Among these, 58 genes were downregulated more than twofold (section III). Further analysis suggested that 12 genes among those in section III, including *ABCF2*, *CAP1*, *FAM122B*, *HMG2*, *MLL2*, *NES* (*Nestin*), *PRMT5*, *RCC1*, *RIN2*, *TNFRSF12A*, *TUBG1* and *UBE2Q1*, are aberrantly upregulated in cancer according to the ONCOMINE database (section IV) (Figure 2a and Supplementary Figure 5). To verify the identification of these 12 genes in section IV, we analyzed their mRNA levels by qRT-PCR and found that *ABCF2*, *CAP1*, *NES*, *RCC1*, *TUBG1* and *UBE2Q1* were indeed downregulated by miR-940 (Figure 2b). Of these five genes, *NES* is the only one predicted to have two 7mer-8A binding sites for miR-940 in its 3'-UTR by the Targetscan program (Figure 2a (Section V) and Figure 2c).

To verify that miR-940 targets Nestin, we cloned the full-length Nestin 3'-UTR just after the *Renilla* luciferase reporter gene in psiCHECK-2, which also constitutively expresses the Firefly luciferase gene as an internal control. Co-transfection with miR-940 precursor led to a significant increase in the Firefly/*Renilla* ratio for the Luc-NES-UTR construct, but not for the control Luc construct, suggesting that miR-940 specificity binds to the Nestin 3'-UTR (Figure 2d). Furthermore, the

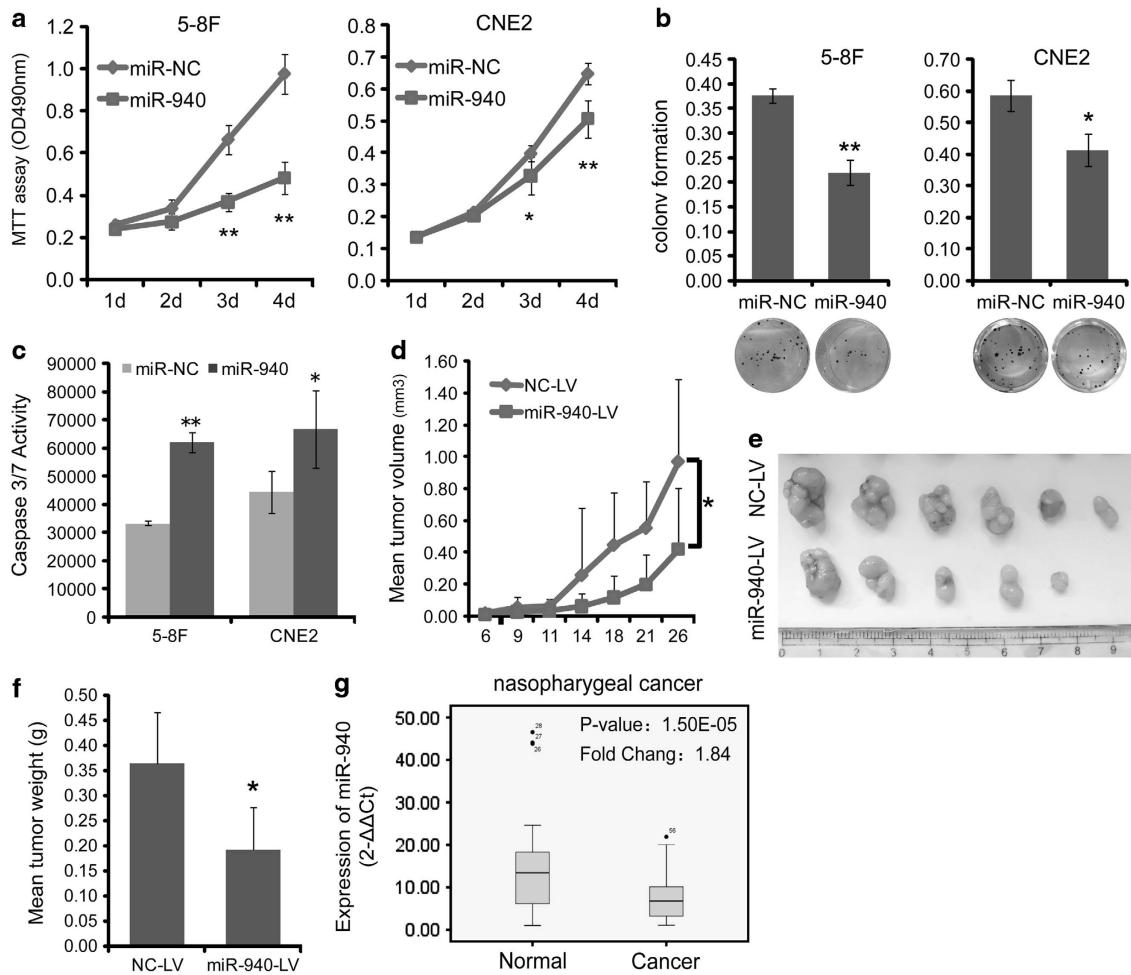


Figure 1 MiR-940 functions as a tumor suppressor. (a–c) 5-8F and CNE2 cells transfected with 30 nM miR-940 precursor (miR-940) or negative control miRNA (miR-NC) were subjected to (a) MTT assay at different timepoints; (b) colony formation assay; and (c) caspase 3/7 activity analysis after 48 h. Data are shown as mean \pm S.D. from three independent experiments. * $P < 0.05$, ** $P < 0.01$, versus miR-NC. Representative plates from colony assays are shown (b, bottom panels). (d–f) 5-8F cells transduced with a miR-940-expressing virus (miR-940-LV) or a negative control virus (NC-LV) were inoculated subcutaneously into the flanks of nude mice ($n = 6$). (d) The average volume of tumors (mean \pm S.E.) was measured using calipers over a time course as shown. (e) The mice were euthanized 26 days after inoculation and the tumors were excised. Tumors from each of the six NC-LV-transduced mice and five of the miR-940-LV-transduced mice are shown. The sixth miR-940-LV-transduced mouse failed to produce a tumor. (f) Tumors from each group were weighed immediately after removal. The average tumor weight is indicated as mean \pm S.E. * $P < 0.05$, compared with negative control. (g) The expression of miR-940 in NPC tissues (cancer) is compared with the expression in matched normal tissues (normal). Mature miR-940 was quantified by qRT-PCR using specific primers for miR-940 and normalized to U6 snRNA expression. Data are shown as $2^{-\Delta\Delta C_t}$ values as a box plot. $n = 28$, $P = 1.50E - 05$, compared with normal tissues

protein levels of Nestin in 5-8F and CNE2 cells were also significantly downregulated by the overexpression of miR-940 (Figure 2e). To verify the specificity of this interaction, we also screened Nestin-targeting miRNAs through Targetscan, miRanda, miRBase and microRNA databases. Twenty-six miRNAs either were found by two or more databases or had two binding sites on the 3'-UTR of Nestin. Among them, miR-125b, miR-650, miR-658 and miR-940 inhibited *Renilla* luciferase activity more than twofold, leading to an increase in the Firefly/*Renilla* ratio (Supplementary Figure 6A); however, only miR-940 inhibited Nestin protein levels in 5-8F cells (Supplementary Figure 6B). Moreover, the relative abundance of miR-940, but not the other three miRNAs, was lower in four NPC cell lines compared with the non-tumorigenic cell line NP69 (Supplementary Figure 6C). Collectively, these

data suggest that miR-940 modulates the expression of a number of genes that are involved in several important pathways, with Nestin comprising a novel target that is directly regulated by miR-940.

Nestin has an important role in promoting tumorigenesis.

Nestin is reported to be modulated according to the grade of malignancy for gliomas.²² To investigate a potential link of Nestin to malignancy in NPC cells, we analyzed Nestin expression in the NPC cell lines 5-8F, 6-10B, CNE1 and CNE2,^{10,11} as well as the glioma cell line U251 as a positive control and the non-transformed nasopharyngeal epithelial cell line NP69 as a negative control. Nestin could be detected in U251, 5-8F, 6-10B and CNE2 cells, which have a low grade of differentiation and a high grade of tumorigenicity,

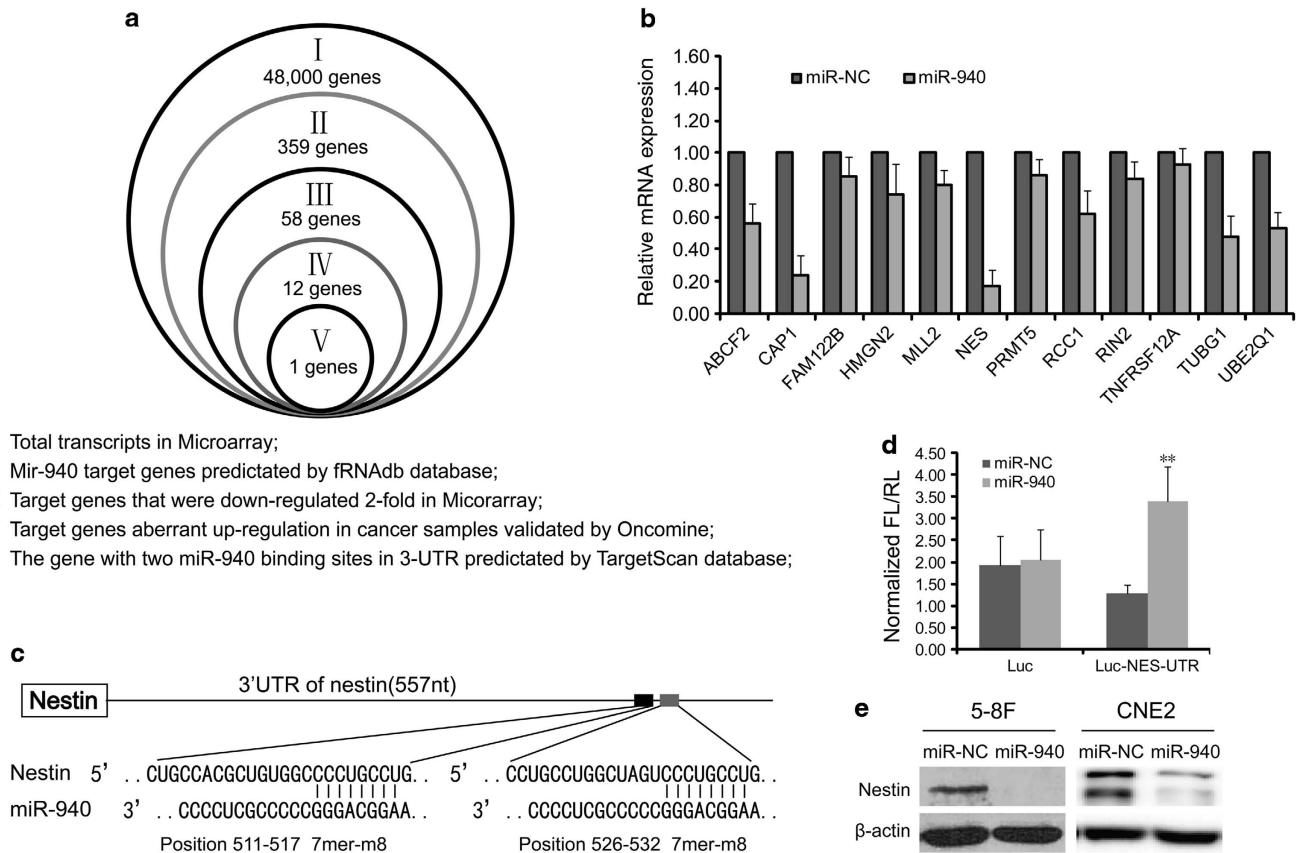


Figure 2 Mir-940 regulates Nestin expression by directly binding its 3'-UTR. (a) Flow diagram depicting the process used to select relevant miR-940 target genes. Each of the circles represents a genes data set (sections I to V), and the numerals represent the number of genes in each section. Genes were selected according to the screening conditions indicated. (b) Relative mRNA levels of the 12 predicted miR-940 target genes from section IV were measured by qRT-PCR following 24 h transfection of miR-940 precursor into 5-8F cells using specific primers. Values are standardized to 18S rRNA expression and normalized to 1.0 in cells transfected with NC. (c) Schematic diagram showing two putative miR-940 binding sites in the Nestin 3'-UTR, as identified by TargetScan. (d) 293T cells were co-transfected with a control psiCHECK-2 vector (Luc) or a psiCHECK-2 plasmid with the Nestin 3'-UTR cloned downstream of the Renilla luciferase reporter gene (Luc-NES-UTR). The cells were also transfected with the miR-940 precursor (miR-940) or a negative control (miR-NC). The vector psiCHECK-2 also contains a Firefly luciferase gene as an internal control. The Firefly/Renilla ratio thus serves as a measure of the inhibition of Renilla expression due to the cloned 3' UTR. Each experiment was repeated at least three times in triplicate. $**P < 0.01$, compared with miR-NC. (e) Ectopic expression of miR-940 reduces Nestin protein levels in 5-8F and CNE2 cells. Cells were transfected with either miR-940 precursor (miR-940) or negative control (miR-NC) for 48 h and subjected to western blotting with the indicated antibodies. Results are representative of three independent experiments

but not in the highly differentiated NPC cell line CNE1 or the NP69 cells, suggesting that Nestin expression may be modulated according to the state of malignancy of NPC cells (Supplementary Figure 7).

Accordingly, we selected the 5-8F and CNE2 cell lines to knockdown endogenous Nestin using an shRNA-based lentivirus (Supplementary Figures 8A and B). Knockdown of Nestin suppressed cell proliferation (Figures 3A and B). Furthermore, Nestin depletion promoted an accumulation of the G2-phase cells at 24 h after synchronization in serum-free medium (Supplementary Figure 9A) and increased the percentage of apoptotic cells to 75–83.5% at 24 h (Supplementary Figure 9B). Moreover, suppression of Nestin obviously increased caspase-3/7 activity for both 5-8F and CNE2 cells (Figure 3C). To verify the *in vivo* function of Nestin in NPC cells, Nestin-knockdown or control cells were subcutaneously inoculated into nude mice. As shown, Nestin-knockdown tumors were significantly smaller than control tumors (Figures 3D–F). We further analyzed Nestin

mRNA levels from 28 paired NPC patient tissues and corresponding adjacent normal tissues and found that the average Nestin mRNA levels were 1.75-fold higher in NPC tissues than in adjacent normal tissues ($P = 1.06E - 06$) (Figure 3G). To examine the relationship between Nestin expression and miR-940 expression, we compared Nestin and miR-940 RNA expression in the same NPC samples. As shown in Figure 3H, a significant inverse correlation was observed ($R = -0.43$; $P < 0.001$). Parallel immunohistochemical staining of Nestin and *in situ* hybridization of miR-940 verified their inverse correlation in nasopharyngitis and NPC sections (Figure 3I). These data indicate that miR-940 downregulation is associated with the increased Nestin protein levels in NPC. Interestingly, we also found that Nestin is located both in the nucleus and cytoplasm of tumor cells in NPC sections (Supplementary Figure 10), which suggests the possibility that translocation of Nestin from the cytoplasm to the nucleus may contribute to the tumorigenesis of NPC.

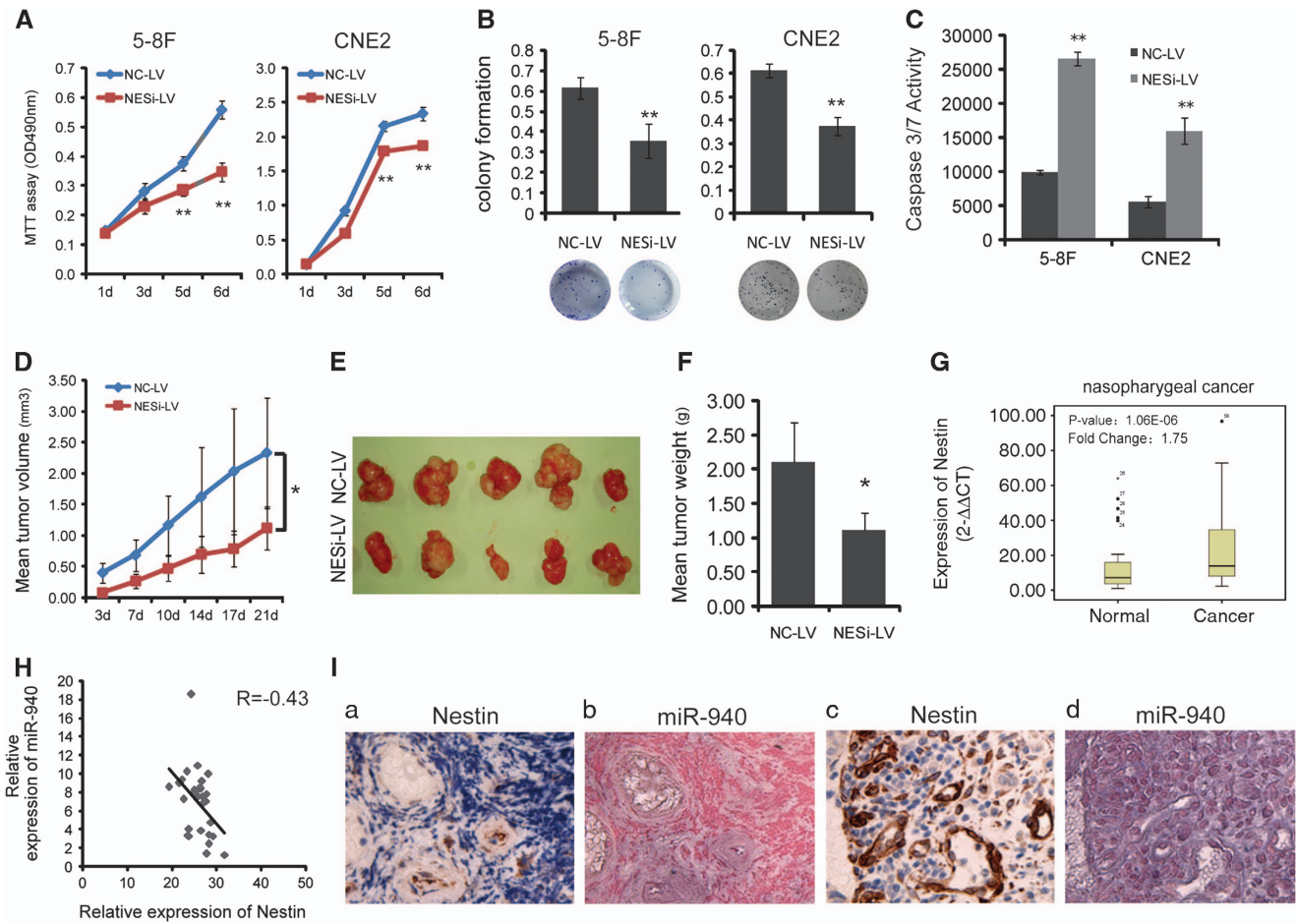


Figure 3 Nestin expression is associated with tumorigenicity. (A–C) 5-8F and CNE2 cells were transduced with sh-Nestin (NESi-LV) or negative control (NC-LV) lentivirus and then were subjected to (A) MTT assay at different timepoints; (B) colony formation assay; and (C) caspase activity analysis at 48 h after seeding. Representative plates from colony assays are shown (B, bottom panels). (D–F) 5-8F cells transduced with sh-Nestin (NESi-LV) or negative control (NC-LV) lentivirus were inoculated subcutaneously into the flanks of nude mice ($n = 5$). (D) The average volume of tumors (mean \pm S.E.) was measured using calipers over a timecourse as shown. (E) The mice were euthanized and the tumors were excised 21 days after inoculation. Tumors from each of the five NC-LV-transduced and NESi-LV-transduced mice are shown. (F) Tumors from each group were weighed immediately after removal. The average tumor weight is indicated as mean \pm S.E. * $P < 0.05$, compared with NC-LV. (G) The expression of Nestin was measured by qRT-PCR in NPC patient tissues compared with normal tissues. Data are shown as $2^{-\Delta\Delta C_t}$ values relative to 18S rRNA expression in box plots. $n = 28$, $P = 1.06E - 06$, compared with normal tissues. (H) The expression of miR-940 was inversely correlated with Nestin expression in NPC tissues ($R = -0.43$; $P < 0.001$). Expression levels in each of 28 NPC patient samples were determined by qRT-PCR. Nestin mRNA levels were normalized to 18S rRNA and miR-940 levels were normalized to U6. For comparison, a two-tailed, unpaired t -test was used. (i) Representative images showing inverse expression of miR-940 (by *in situ* hybridization) and Nestin (by immunohistochemistry) in (a, b) nasopharyngitis and (c, d) poorly differentiated NPC sections. Magnification: $\times 400$. (a) Negative expression of Nestin. (b) Positive expression of miR-940. (c) Positive expression of Nestin. (d) Negative expression of miR-940

To determine whether Nestin expression may contribute to other types of cancer, we evaluated its expression using the Oncomine database. This analysis showed that Nestin is also highly upregulated in the brain and CNS cancer,^{23,24} colon,²⁵ esophageal²⁶ and gastric cancer²⁷ (Supplementary Figure 11). To verify Nestin function in diverse cell types, we compared Nestin mRNA levels in esophageal cancer cell lines EC-1, EC-9706, KYSE-150 and TE-1; liver cancer cell lines MHCC97-H and QGY-7701; and glioma cell line U251 (Supplementary Figure 12A). Depletion of Nestin in TE-1, MHCC 97-H, QGY-7701 and U251 cells, which showed equal or higher Nestin expression compared with 5-8F cells, also suppressed cell proliferation, suggesting that Nestin has a common role in regulating cell proliferation in different types of cancer cells (Supplementary Figures 12B–D).

MiR-940 inhibits cell proliferation and promotes apoptosis by targeting Nestin. To test the hypothesis that miR-940 regulates cell proliferation and apoptosis by targeting Nestin, 5-8F cells were co-transfected with miR-940 precursor and Nestin-expressing vector. As shown in Figure 4a, Nestin expression increased cell proliferation. Furthermore, overexpression of miR-940 inhibited cell proliferation, whereas this inhibition was partially reversed by coexpression of Nestin. Consistently, Nestin and miR-940 had opposite effects on the levels of apoptosis, and the enhanced apoptosis by miR-940 was reversed by co-transfection of Nestin (Figure 4b). A similar pattern of caspase-3/7 activity in transfected cells verifies these results (Figure 4c). The observation that the suppression of cell proliferation and activation of apoptosis induced by miR-940

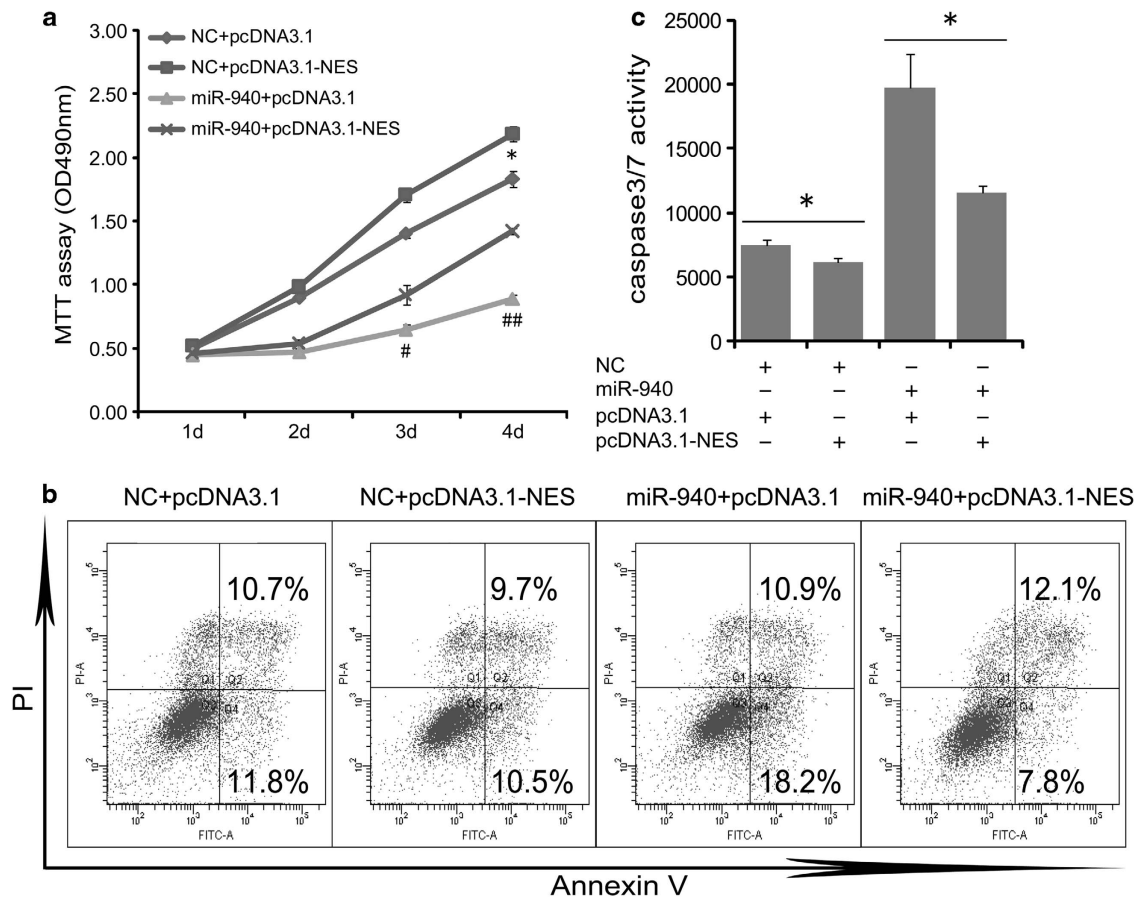


Figure 4 MiR-940 inhibits cell proliferation and promotes apoptosis by targeting Nestin. 5-8F cells were transfected with miR-940 precursor (miR-940) or control miRNA (NC), together with Nestin overexpression plasmid (pcDNA3.1-NES) or control plasmid (pcDNA3.1). (a) The cells were subjected to MTT analysis at different time points following transfection. Data are shown as mean \pm S.D. from three independent experiments. * $P < 0.05$, compared with NC + pcDNA3.1; ## $P < 0.01$, compared with miR-940 + pcDNA3.1. (b) Twenty-four hours after transfection, cells were harvested and analyzed by PI/Annexin V staining and flow cytometry. (c) Caspase 3/7 activity in 5-8F cells was measured 48 h after co-transfection. * $P < 0.05$, compared with respective control

can be reversed by overexpression of Nestin suggests that the effects of miR-940 on cell growth and survival are largely mediated by its effects on Nestin.

Nestin depletion induces spontaneous DNA damage accumulation and increases IR sensitivity of NPC cells.

To further examine the molecular mechanism of Nestin in promoting proliferation and activating tumorigenesis, we performed a phospho-specific cell cycle protein antibody array (Full Moon BioSystems Inc., Sunnyvale, CA, USA; PCC238). Knockdown of Nestin resulted in a decrease in the phosphorylation of FOXO1 Ser319, cyclin-dependent kinase 5 (CDK5) Ser780, GSK-3 β Ser9, Rb Ser780, 795 and 807, each of which are regulators of cell cycle. In addition, knockdown of Nestin led to an increase in the phosphorylation levels of BRCA1 Ser1423, Chk1 Ser317, SMC1 Ser957, NBS1 Ser343 and c-Abl Tyr412, each of which are involved in DNA damage response (DDR) and repair^{28,29} (Supplementary Table 2). These results suggest a pathway of cell cycle regulation and DDR that is associated with Nestin-dependent tumorigenesis.

The genome is constantly exposed to environmental and endogenous genotoxic insults that challenge its structural

integrity. Spontaneous DNA damage occurs at a rate of 10 000 lesions per cell per day.³⁰ Given the effects of Nestin knockdown on the phosphorylation of cell cycle and DDR proteins, we proposed that Nestin depletion might lead to the accumulation of spontaneous DNA damage. To assess this possibility, we measured the expression of γ H2AX, a marker for DNA double-strand breaks (DSBs) in 5-8F cells. Knockdown of Nestin increased levels of γ H2AX both before and after treatment with doxorubicin (Dox), a chemotherapy drug that can induce DSBs (Figures 5a and b). These data confirm that Nestin depletion both lead to the accumulation of spontaneous DNA damage and enhances the DNA damage induced by a cytotoxic agent in 5-8F cells.

To verify the role for Nestin in DDR, we performed alkali comet assays using IR-exposed 5-8F cells. As shown in Figures 5c and d, Nestin-depleted cells showed more DNA damage than control cells in the absence of IR. Moreover, the levels of IR-induced DNA damage remained higher at 4 h in the Nestin-knockdown cells but returned to basal levels at 6 h. These results verify that spontaneous DNA damage is accumulated in Nestin-knockdown cells and that Nestin participates in the DNA damage repair process after DNA damage induction.

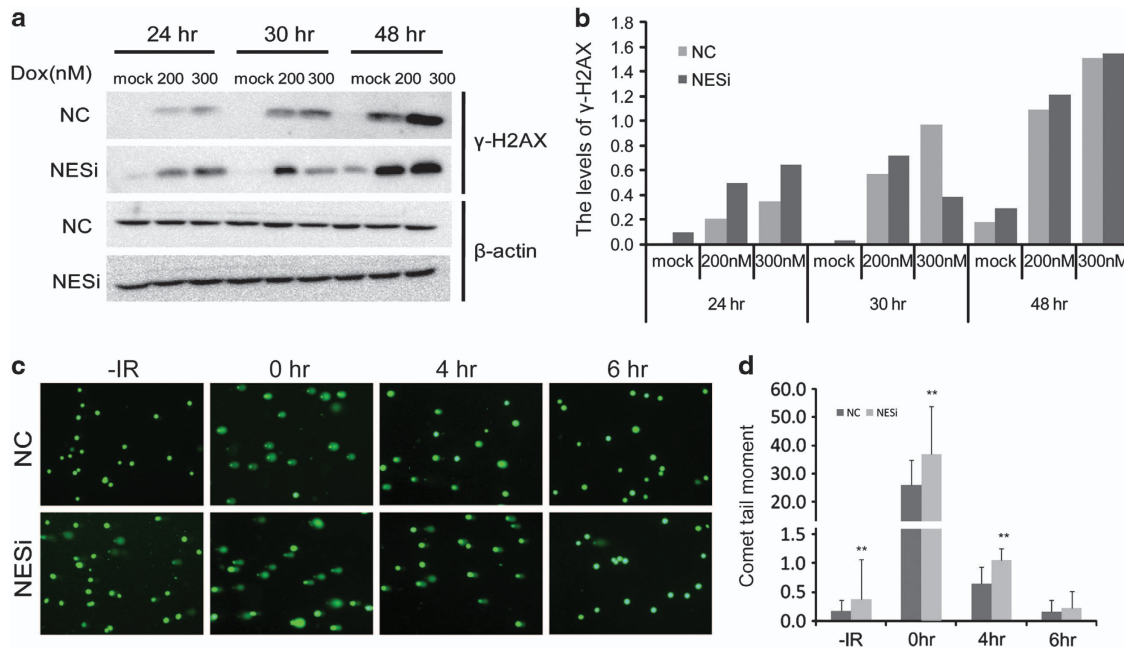


Figure 5 Nestin depletion suppresses DNA damage repair and increases IR sensitivity. (a) Nestin-depleted (NESi) or control (NC) 5-8F cells were treated with the indicated concentrations of doxorubicin (Dox). After 24 h, Dox was removed and cells were cultured in fresh medium for the indicated time periods. The protein levels of γ -H2AX were examined by western blotting. β -Actin was tested as a loading control. (b) Quantification of the levels of γ -H2AX protein from panel a. Values were normalized to β -actin. (c) 5-8F/NC and 5-8F/NESi cells were exposed to 4 Gy of IR, and subjected to alkaline comet analysis at the indicated time points. Magnification: $\times 100$. (d) Quantification of tail moments from panel c. Tail moments for each condition was calculated on a minimum of 100 cells for each data point

To further determine whether the effects of Nestin on the cell cycle distribution are maintained in the presence of increasing doses of radiation, control and Nestin-knockdown cells were exposed to a range of doses of IR. Increasing doses of radiation resulted in the accumulation of cells in the G2 phase for both Nestin-knockdown and control cells; however, Nestin-knockdown cells displayed more obvious effects than control cells on G2 arrest with 4 Gy radiation after 24 h (85.77% versus 71.08%). Additionally, the G2 arrest was maintained in Nestin-knockdown cells after 48 h for both the 4 and 6 Gy dose 77.96% versus 33.64% at 4 Gy; 72.24% versus 40.06% at 6 Gy. The delay of cell cycle re-entry caused by Nestin depletion strongly supports our hypothesis that Nestin depletion sensitizes cells to radiotherapy and suppresses DNA damage repair (Supplementary Figure 13).

Nestin depletion enhances the effects of IR on the suppression of xenograft tumor formation. Based on the above results, we speculated that a combination of Nestin depletion and IR should inhibit tumor growth more effectively. To test this possibility, we subcutaneously inoculated control cells or Nestin-depleted 5-8F cells into nude mice. Subsequently, the mice were exposed to 0, 4, 8, 12 or 16 Gy of IR at 21 days after inoculation. The mean volume of tumors generated by Nestin-depleted cells was obviously smaller than that of the control (Figure 6a), and at day 27, the Nestin-knockdown tumors were significantly smaller than the control tumors (Figures 6b and c). Furthermore, the control and Nestin-knockdown tumors were markedly smaller when treated with IR. These results suggest that Nestin depletion and IR function synergistically to reduce tumor growth.

To determine the functional effect of Nestin depletion, survival rates were calculated after IR treatment. The survival rate of mice was improved by Nestin knockdown after exposure to 4, 8 or 12 Gy dose of radiation (Figure 6d). These results confirm that Nestin knockdown and IR treatment function synergistically to suppress xenograft tumor formation.

Discussion

We have demonstrated for the first time that miR-940 functions as a novel tumor suppressor in NPC. MiR-940 inhibits NPC cell proliferation, arrests cell cycle, induces apoptosis through the activation of caspase-3/7 and inhibits xenograft tumor formation. Furthermore, miR-940 functions by targeting Nestin, and consistently, depletion of Nestin has similar functional effects as miR-940 overexpression. In support of the role of Nestin in mediating the effects of miR-940, suppression of cell proliferation and induction of apoptosis by miR-940 was rescued by overexpression of Nestin. It is well known that miRNAs act within a complex network of regulation, and it is formally possible that Nestin may be regulated by additional miRNAs. However, our data suggest that miR-940 is a key regulator of Nestin that contributes to tumorigenesis in NPC.

Interactions between selected kinases and intermediate filaments appear instrumental in regulating signaling toward apoptosis.^{31,32} Acting as a scaffold protein for the Cdk5/p35 complex, Nestin regulates the activity of Cdk5 and its regulator p35 to promote the survival of neuronal progenitor cells facing oxidative stress. Retention of the Cdk5/p35

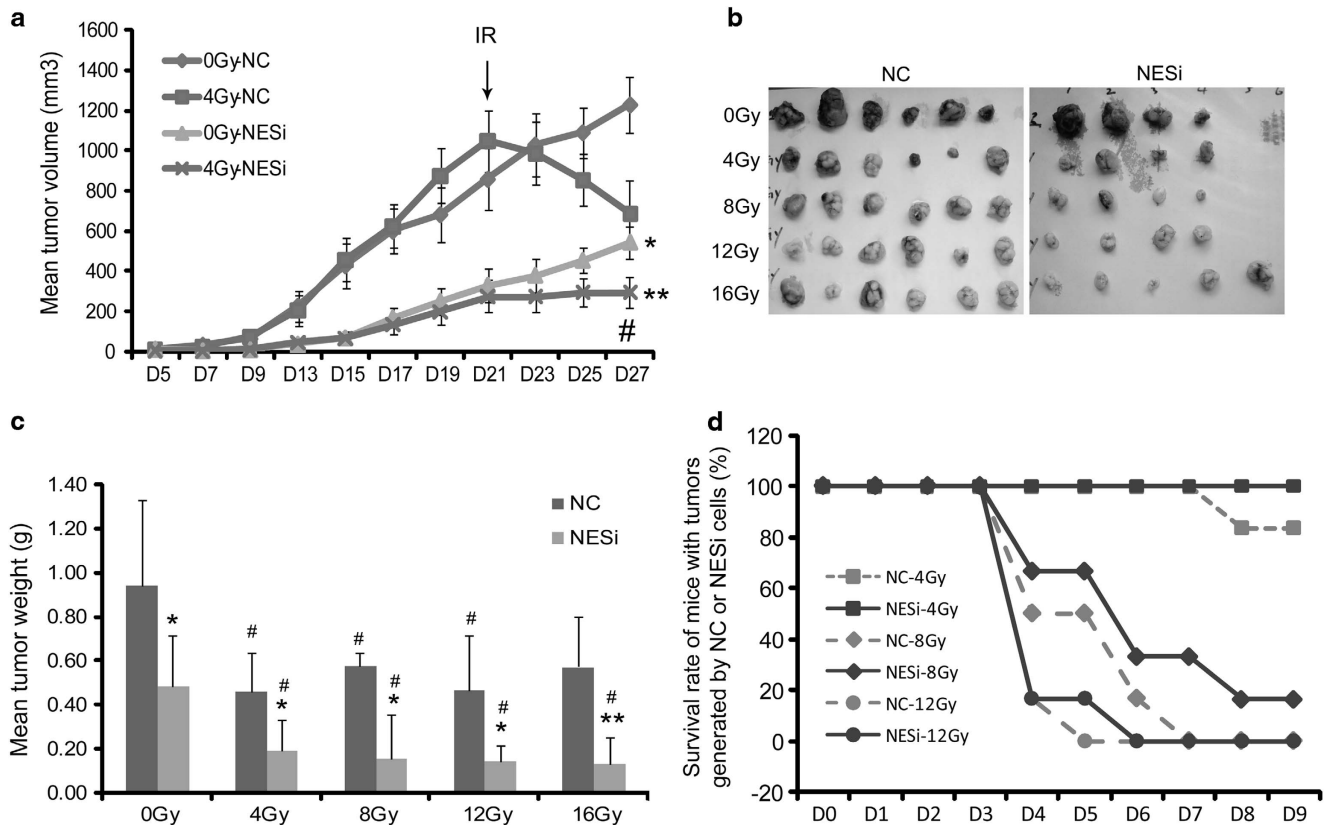


Figure 6 Suppression of tumor growth and survival after γ -radiation is enhanced by Nestin knockdown. 5-8F/NC and 5-8F/NESi cells were inoculated subcutaneously into nude mice ($n = 6$). At 21 days after inoculation, the mice were exposed to the indicated doses of γ -radiation. (a) The average volume (mean \pm S.E.) of tumors in nude mice was measured using calipers. * $P < 0.05$ for NESi compared to control; # $P < 0.05$ for 4 Gy compared to 0 Gy. (b) At 27 days after inoculation, the mice were euthanized and the tumors were excised. Tumors from each of the 5-8F/NC mice and five or six of the 5-8F/NESi-inoculated mice are shown. (c) The average weight of tumors (mean \pm S.E.) was uniformly reduced for 5-8F/NESi cells. * $P < 0.05$ for NESi compared to control; # $P < 0.05$, compared to 0 Gy. (d) Nestin knockdown affects the survival rate of nude mice in response to IR. The survival rate is shown for nude mice inoculated with 5-8F/NC or 5-8F/NESi cells and then exposed to 4, 8, and 12 Gy at different days after radiation

complex in the cytoplasm by Nestin increases the stability of p35 and reduces the generation of p25.³³ Consistent with these findings, our data indicate that Nestin depletion induces apoptosis in the NPC cell lines 5-8F and CNE2. As expected, gene microarray analysis shows that Cdk5 is downregulated twofold when Nestin is depleted (data not shown). This indicates that Nestin may engage in a similar mechanism in terms of regulating Cdk5/p35 activity to protect tumor cells from apoptosis and increase resistance to IR.

Accumulating evidence suggests that Cdk5 participates in DNA damage signaling through modification of DNA damage proteins, such as PARP, ATM and APE1.^{34–37} Cdk5 silencing sensitizes non-neuronal cells to DNA-damaging agents, leading to the spontaneous formation of DSBs and activation of markers of DSB repair. In addition, Cdk5 is necessary for the activation of the intra-S and G2/M cell-cycle checkpoints.³⁴ Depletion of Cdk5 reduces the recruitment and persistence of PARP-1, a single-stranded break repair protein, at sites of DNA damage after exposure to IR.³⁷ However, Cdk5-depleted cells still can repair single-stranded breaks, probably via the long patch base-execution repair pathway, suggesting that the enhanced radiation sensitivity of Cdk5-knockdown cells involves the role of Cdk5 in other pathways. Our findings indicate that depletion of Nestin leads

to increased spontaneous DNA damage and delay of the DDR. These results suggest that depletion of Nestin may reduce Cdk5 expression, resulting in eventual G2/M arrest. We also provided evidence that Nestin depletion increases the levels of spontaneous DNA damage and IR sensitivity both *in vitro* and *in vivo*, which provides additional confirmation of a role for Nestin in DSB repair.

Interaction with the Cdk5/p35 complex may be the one of the mechanisms by which Nestin participates in DNA damage repair, which highlights the scaffold functions of Nestin as a cytoplasmic intermediate filament protein. However, we observed Nestin in both the nucleus and cytoplasm of tumor cells in NPC sections. Consistent with our findings, Nestin has been detected in the nuclei of neuroblastoma,^{21,38} glioblastoma multiforme,^{39,40} angiosarcoma cells⁴¹ and non-small-cell lung cancer.⁴² Furthermore, Nestin binds DNA in the nuclei of N-myc-amplified neuroblastoma cell lines.²¹ It has been suggested that translocation of depolymerized Nestin in the cytoplasm is mediated by binding to Cdk5 and Cdc2 kinases, which carry nuclear localization signals and also regulate Nestin assembly during mitosis by phosphorylation of its C terminus.^{21,38} Consistent with a role for Nestin in the nucleus, other cytoplasmic intermediate filaments bind specific DNA sequences in the nucleus^{43–45} and influence

DNA organization and chromatin structure.⁴⁶ For example, overexpression of vimentin in melanomas or keratin in breast carcinomas leads to increased tumor cell motility and invasiveness.⁴³ Based on our findings and this additional evidence, we speculate that the translocation of Nestin in tumor cell nuclei may facilitate the participation either in chromatin organization or the DDR. However, additional studies are needed to provide a detailed mechanism to characterize the function of miR-940 and Nestin in the DDR.

In conclusion, our data show that miR-940 suppresses cell proliferation and promotes apoptosis in NPC cells by directly regulating its target gene *Nestin*, an oncogene that promotes cell proliferation and protects tumor cells against apoptosis and IR. We also revealed an important role in the DDR for Nestin. However, many questions remain to be answered, such as how Nestin participates in the DDR, whether accumulation of spontaneous DNA damage induced by Nestin depletion is related with Cdk5-mediated DNA damage signaling, and whether translocation into the nucleus allows Nestin to participate in the DDR directly.

Materials and methods

Patient samples and cell lines. Pair-matched tumors and adjacent non-tumor nasopharyngeal tissues from 28 patients undergoing resection for nasopharyngeal cancer were obtained from the Department of Pathology, Sun Yat-sen Memorial Hospital, Sun Yat-sen University (Guangzhou, People's Republic of China). NPC cell lines 5-8F, 6-10B, NP69, CNE1 and CNE2 were kindly provided by Professor Kaitai Yao (Cancer Research Institute, Southern Medical University, Guangzhou, China). The 293T, TE-1, QGY-7701 and U251 cell lines were obtained from the Chinese Academy of Science cell bank (Shanghai, China). EC-1, EC-9706, KYSE-150 and MHCC97-H cells were kindly provided by the Central Laboratory, Tongji University Affiliated People's 10th Hospital (Shanghai, China). The 5-8F, 6-10B, U251, CNE1, CNE2, EC-1, EC-9706, KYSE-150 and TE-1 cell lines were maintained at 37 °C in an atmosphere of 5% CO₂ in RPMI-1640 supplemented with 10% fetal bovine serum (Invitrogen Corp., Carlsbad, CA, USA) in 25-ml culture flasks. The 293T, MHCC97-H and QGY-7701 cell lines were maintained in DMEM/high glucose (Invitrogen) with 10% fetal bovine serum. The immortalized nasopharyngeal epithelial cell line NP69 was cultured in keratinocyte serum-free medium (Invitrogen) supplemented with 25 µg/ml bovine pituitary extract and 0.2 ng/ml recombinant epidermal growth factor, as suggested by the manufacturer.⁴⁷

Stable infection. For stable miR-940 stable overexpression, 5-8F cells were infected with lentivirus expressing miR-940 (Genchem Limited Company, Changzhou, China) or its negative control at 30–50% confluency. A monoclonal population of stably infected cells was prepared by limiting dilution assay, and an miR-940-overexpressing clone was selected by qRT-PCR. Lentivirus stably expressing shRNA targeting Nestin or its negative control were introduced into 5-8F and CNE2 cells by analogous methods. Both qRT-PCR and western blots were performed to verify functional expression.

Real-time PCR analysis. Total RNA from patient tissue samples and cell lines was extracted using TRIzol reagent (Invitrogen) following the manufacturer's protocol. RNA concentrations and quality were determined by spectrophotometry (Eppendorf, Hamburg, Germany) and gel analysis. Forward and reverse primer pairs were designed for Nestin and 18S rRNA as follows: Nestin-Q-PCR (forward: 5'-GGAAGAGTCTGACCCTGT-3'; reverse: 5'-AGACTAGCGGCATTCCT-3') and 18S rRNA Q-PCR (forward: 5'-CCTGGATACCGCAGCTAGGA-3'; reverse: 5'-GCGGCGCAATACGAATGCC-3'). Reverse transcription was performed using the PrimeScript™ RT-PCR Kit (Takara Bio Inc, Otsu, Shiga, Japan). The expression of mature miRNAs was assayed using the miRCURY LNA Universal RT microRNA PCR cDNA Synthesis Kit (Exiqon, Vedbæk, Denmark) with specific primers for hsa-miR-940 or U6 snRNA as a control (Exiqon). Reverse transcription was performed using 1 µg of total RNA according to the mercury LNA

SYBR Green Master Mix Kit (Exiqon) protocol and measured with an ABI7900 Real-Time PCR Detection System (Applied Biosystems, Foster city, CA, USA). The $\Delta\Delta C_t$ method for relative quantization was used to determine gene expression.

Immunohistochemistry. Primary antibodies against Nestin (1 : 400 dilution; Merck, Darmstadt, Germany) were used in our study. Briefly, tissue sections were treated with xylene and graded alcohol and then equilibrated in PBS. Antigen retrieval was performed by microwaving the slides for 15–20 min in a buffer containing 10 mM sodium citrate (pH 6.0). Endogenous peroxidase was blocked by incubating the slides in methanol containing 3% H₂O₂ at room temperature for 10 min. Nonspecific binding was blocked by incubating with normal goat serum (Invitrogen) for 30 min at room temperature, and then sections were incubated with anti-Nestin antibody (1 : 300 dilution) for 1 h at room temperature. Slides were washed several times in PBS and incubated with biotinylated anti-mouse IgG (1 : 100 dilution) for 30 min at room temperature, followed by peroxidase-labeled streptavidin (1 : 200 dilution; Sigma-Aldrich, St. Louis, MO, USA) for 30 min at room temperature. The antigen was visualized by incubation for 10–20 min at room temperature with diaminobenzidine tetrahydrochloride according to the manufacturer's instructions.

In situ hybridization. *In situ* hybridization was performed on formalin-fixed, paraffin-embedded sections (5 µm) of nasopharyngitis and NPC tissue. Briefly, after dewaxing, sections were treated with proteinase K (2 µg/ml) at 37 °C for 15 min, washed and prehybridized for 1 h at 49 °C. Hybridization with digoxigenin (DIG)-labeled miRCURY LNA probes (Exiqon) was performed overnight at 49 °C. Slides were then washed at 49 °C and incubated with alkaline phosphatase-conjugated anti-DIG Fab fragments (1 : 1500; Roche Applied Science, Indianapolis, IN, USA) for 1 h at room temperature. The staining was visualized by adding BM purple AP substrate (Roche Applied Science) according to the manufacturer's instructions.

Western blotting. After transfection and/or treatment, cells were subjected to western blotting with anti-Nestin (1 : 500; Merck), anti- γ H2AX (1 : 1000; Cell Signaling, Beverly, MA, USA) or β -actin (1 : 1500; Santa Cruz Biotechnology Inc, Dallas, TX, USA) antibodies. Cells were harvested and lysed in 0.5 ml of lysis buffer (10 mM Tris-HCl, pH 7.6, 5 mM EDTA, 50 mM NaCl, 30 mM sodium pyrophosphate, 50 mM NaF, 0.1 mM Na₂VO₄, 1% Triton X-100, 1 mM phenylmethylsulfonyl fluoride and protease inhibitor cocktail (Roche Applied Science)). Protein (20 µg) was separated by SDS-PAGE on 10% gels. The proteins were electrophoretically transferred to PVDF membranes (Millipore, Billerica, MA, USA) and incubated with primary antibody, followed by incubation with an HRP-conjugated secondary antibody (Santa Cruz Biotechnology Inc). After washing with TBS, the bound antibodies were visualized by enhanced chemiluminescence (Pierce, Rockford, IL, USA) and recorded on X-ray films.

Xenograft tumor model. Animal experiments were conducted in accordance with the Guide for the Care and Use of Animals for research purposes. Female athymic nude nu/nu mice (3–4 weeks old) were purchased from Shanghai Laboratory Animal Co Ltd (SLAC, Shanghai, China). The mice were bred and maintained under specific pathogen-free conditions in the Animal Facility, Cancer Research Institute, Southern Medical University (Guangzhou, China). For Nestin-knockdown experiments, 5-8F/NC or 5-8F/NESi cells (1 × 10⁶ cells) were inoculated subcutaneously into the right flanks of nude mice. For miR-940 overexpression experiments, 5-8F/miR-940-LV and 5-8F/NC-LV cells were similarly inoculated into nude mice. The volume of the implanted tumor was measured every 4 days with a vernier caliper, using the formula: $V = L \times W^2/2$, where V is the volume (mm³); L is the biggest diameter (mm); W is the smallest diameter (mm). The mice were killed and the tumors were weighed 3 weeks after inoculation.

Luciferase reporter assay. The human 3'-UTR of the *NES* gene was amplified by PCR using the following primers: Nestin-3'-UTR-Forward (5'-ATCGCTCGAGGAGGACTAGGAAAGACCATC-3') and Nestin-3'-UTR-Reverse (5'-ATCGGCGGCCGCGGAGGCATTACTTTATTC-3'). The cDNA was cloned into the *XhoI/NotI* site of the psiCHECK2 vector (Promega, Madison, WI, USA), downstream of the *Renilla* luciferase gene, to generate the vector psiCHECK2-NES-3'-UTR. For the luciferase reporter assay, 293T cells (5 × 10⁴ cells per well) were seeded in 24-well plates 24 h before transfection. Cells were co-transfected

with 0.5 μ g of the psiCHECK2-NES-3'-UTR plasmids together with 50 nM of miRNA precursor molecule (Ambion, Foster City, CA, USA) or 50 nM of negative control miRNA (Ambion) using Lipofectamine 2000 (Invitrogen). Firefly and *Renilla* luciferase activities were measured by using a dual-luciferase reporter assay (Promega) 24 h after transfection. The Firefly/*Renilla* ratio was calculated as a measure of *Renilla* inhibition by the cloned 3'-UTR.

Cell proliferation assay. To determine the effect of Nestin on the proliferation of NPC cell lines, 5-8F and CNE2 cells (2.5×10^5 cells per well) were transfected with pre-miR miR-940 precursor molecule or pre-miR miRNA precursor molecule as a negative control (Ambion) using Lipofectamine 2000 (Invitrogen) in a 6-well plate according to the manufacturer's protocol. Then, these transfected cells (1×10^3 cells per well) were seeded into 96-well plates. MTT assays were performed at days 1–7. The absorbance of the samples was measured with a spectrophotometer reader at 490 nm. Each assay was performed in triplicate and repeated three times independently.

Colony formation assay. Cell lines transfected with synthesized oligonucleotides or vectors were seeded in 12-well plates (100 cells per well) and incubated for 7–10 days to allow colony growth. Colonies were stained with crystal violet, and those containing 50 or more cells were counted. The plating efficiency was calculated by dividing the average number of colonies per dish by the number of cells plated. Survival fractions were calculated by normalization to the plating efficiency of appropriate control groups.

Cell cycle analysis. For cell cycle analysis, parental and transfected cells in the log phase of growth were stained with propidium iodide (PI) and examined with an FACS flow cytometer. DNA histograms were analyzed with modified software. To examine the effect of Nestin suppression on cell cycle, NC and NESi cells were synchronized in serum-free medium for 24 h, and were then harvested at 24 h and analyzed for DNA content by FACS.

Caspase-3/7 assay. Following treatment, cells were seeded into 96-well plates (5×10^3 cells per well). After 48 h of incubation at 37 °C, caspase-3/7 substrates (Promega) were added according to the manufacturer's instructions and plates were incubated for 1 h at 37 °C in the dark. Relative light intensity was measured in each well using a microplate luminometer.

Apoptosis analysis. For apoptosis analysis, the treated cells were harvested after 24 or 48 h, and then stained with PI- and FITC-labeled anti-annexin-V antibody, and analyzed by FACS.

Comet assay. DSBs were measured in 5-8F-treated cells using the OxiSelect Comet Assay system (Cell Biolab, San Diego, CA, USA) according to the manufacturer's instructions. Comet tail moments were scored using the CASP software (CaspLab, Comet Assay Software Project, <http://casplab.com/download>).

cDNA microarray analysis. Total RNA was extracted using TRIzol reagent (Invitrogen) following the manufacturer's protocol. The quality and purity were assessed using an Agilent 2100 bioanalyzer (Agilent, Santa Clara, CA, USA). The criteria for inclusion were RIN ≥ 7 and 28S/18S ≥ 0.7 . Sample labeling and hybridization were performed according to standard procedures using the Illumina BeadChip assay (HumanWG-6_v3; <http://www.Illumina.com>; Illumina, San Diego, CA, USA) to determine the expression of 48 000 genes. Transcripts were considered as 'expressed' only when the average intensity of signals in perfect match samples were 1.5-fold higher than that in mismatch samples, and the differences between the average intensity of signals were fourfold higher than that of experimental noise. Data analysis was performed using Microarray suite 5.0 software (Affymetrix, Santa Clara, CA, USA). T-tests were conducted using MATLAB 7.5 (MathWorks, Natick, MA, USA). The genes were identified and annotated by online databases GO <http://www.geneontology.org>, and GenBank <http://www.ncbi.nlm.nih.gov/Genbank>. Gene set enrichment analysis was performed using EASE software.

Phospho-specific cell cycle protein antibody array analysis. Phospho-specific cell cycle protein antibody array was performed using total lysates obtained from 5-8F/ NC and 5-8F/ NESi cells by Full Moon BioSystems Inc. (Sunnyvale, CA, USA; PCC238) according to the described protocol.⁴⁸ The assay is based on the incubation of biotin-labeled total cell lysates with array slides

on which antibodies are immobilized and the detection of the biotin-labeled protein–antibody complexes by Cy3-streptavidin.

Statistical analysis. Differential expression of miRNA or Nestin in surgical samples was determined by testing the null hypothesis that the mean of log₂-transformed values of fold change was equal to 0 for one-sample t-tests. The Student's t-test was applied to determine the differences between sample means obtained from at least three experiments. Statistical analyses were performed with statistical package for social sciences (SPSS package) version 17.0. All tests of statistical significance were two-sided. $P < 0.05$ was considered to be statistically significant.

Study approval. All animal procedures were performed according to United Kingdom Co-ordinating Committee on Cancer Research (UKCCCR) Guidelines for the Welfare of Animals in Experimental Neoplasia and approved by The Animal Medical Center of Southern Medical University. Informed consent was obtained from all patients for the scientific use of biologic material with approval of the Ethics Committee of Sun Yat-sen Memorial Hospital.

Conflict of Interest

The authors declare no conflict of interest.

Acknowledgements. This work was supported by the National Natural Science Foundation of China (Grant No. 90919050 to AH; Grant No. 81071524 to FS; Grant No. 81301704 to JM) and the National Key Basic Research and Development Program (The 973 Program, Grant No. 2010CB529401 to JA).

Author Contributions

FS, JA, AH and JM conceived and designed the experiments. JM, CL, YZ, WX and ZL performed the experiments. JM, FS, JA and AH analyzed the data. QP, AH and HZ provided material. JA and FS wrote the paper. All authors discussed the results and commented on the manuscript.

- Chang ET, Adami HO. The enigmatic epidemiology of nasopharyngeal carcinoma. *Cancer Epidemiol Biomarkers Prev* 2006; **15**: 1765–1777.
- Lee AW, Yau TK, Wong DH, Chan EW, Yeung RM, Ng WT et al. Treatment of stage IV (A-B) nasopharyngeal carcinoma by induction-concurrent chemoradiotherapy and accelerated fractionation. *Int J Radiat Oncol Biol Phys* 2005; **63**: 1331–1338.
- Le QT, Tate D, Koong A, Gibbs IC, Chang SD, Adler JR et al. Improved local control with stereotactic radiosurgical boost in patients with nasopharyngeal carcinoma. *Int J Radiat Oncol Biol Phys* 2003; **56**: 1046–1054.
- Valencia-Sanchez MA, Liu J, Hannon GJ, Parker R. Control of translation and mRNA degradation by miRNAs and siRNAs. *Genes Dev* 2006; **20**: 515–524.
- Ahmed FE. Role of miRNA in carcinogenesis and biomarker selection: a methodological view. *Expert Rev Mol Diagn* 2007; **7**: 569–603.
- Chen CZ. MicroRNAs as oncogenes and tumor suppressors. *N Engl J Med* 2005; **353**: 1768–1771.
- Croce CM. Oncogenes and cancer. *N Engl J Med* 2008; **358**: 502–511.
- Croce CM. Causes and consequences of microRNA dysregulation in cancer. *Nat Rev Genet* 2009; **10**: 704–714.
- Shi W, Alajez NM, Bastianutto C, Hui AB, Mocanu JD, Ito E et al. Significance of Plk1 regulation by miR-100 in human nasopharyngeal cancer. *Int J Cancer* 2009; **126**: 2036–2048.
- Xia H, Ng SS, Jiang S, Cheung WK, Sze J, Bian XW et al. miR-200a-mediated downregulation of ZEB2 and CTNBB1 differentially inhibits nasopharyngeal carcinoma cell growth, migration and invasion. *Biochem Biophys Res Commun* 2010; **391**: 535–541.
- Zhang L, Deng T, Li X, Liu H, Zhou H, Ma J et al. microRNA-141 is involved in a nasopharyngeal carcinoma-related genes network. *Carcinogenesis* 2010; **31**: 559–566.
- Wong TS, Man OY, Tsang CM, Tsao SW, Tsang RK, Chan JY et al. MicroRNA let-7 suppresses nasopharyngeal carcinoma cells proliferation through downregulating c-Myc expression. *J Cancer Res Clin Oncol* 2011; **137**: 415–422.
- Andressen C, Stocker E, Klinz FJ, Lenka N, Hescheler J, Fleischmann B et al. Nestin-specific green fluorescent protein expression in embryonic stem cell-derived neural precursor cells used for transplantation. *Stem Cells* 2001; **19**: 419–424.
- Sejersen T, Lendahl U. Transient expression of the intermediate filament nestin during skeletal muscle development. *J Cell Sci* 1993; **106**(Part 4): 1291–1300.
- Frojman K, Pelliniemi LJ, Lendahl U, Virtanen I, Eriksson JE. The intermediate filament protein nestin occurs transiently in differentiating testis of rat and mouse. *Differentiation* 1997; **61**: 243–249.

16. Terling C, Rass A, Mitsiadis TA, Fried K, Lendahl U, Wroblewski J. Expression of the intermediate filament nestin during rodent tooth development. *Int J Dev Biol* 1995; **39**: 947–956.
17. Lendahl U, Zimmerman LB, McKay RD. CNS stem cells express a new class of intermediate filament protein. *Cell* 1990; **60**: 585–595.
18. Xue XJ, Yuan XB. Nestin is essential for mitogen-stimulated proliferation of neural progenitor cells. *Mol Cell Neurosci* 2010; **45**: 26–36.
19. Chen HL, Yuh CH, Wu KK. Nestin is essential for zebrafish brain and eye development through control of progenitor cell apoptosis. *PLoS One* 2010; **5**: e9318.
20. Krupkova O Jr, Loja T, Zambo I, Veselska R. Nestin expression in human tumors and tumor cell lines. *Neoplasma* 2010; **57**: 291–298.
21. Thomas SK, Messam CA, Spengler BA, Biedler JL, Ross RA. Nestin is a potential mediator of malignancy in human neuroblastoma cells. *J Biol Chem* 2004; **279**: 27994–27999.
22. Dahlstrand J, Collins VP, Lendahl U. Expression of the class VI intermediate filament nestin in human central nervous system tumors. *Cancer Res* 1992; **52**: 5334–5341.
23. Bredel M, Bredel C, Juric D, Harsh GR, Vogel H, Recht LD *et al*. Functional network analysis reveals extended gliomagenesis pathway maps and three novel MYC-interacting genes in human gliomas. *Cancer Res* 2005; **65**: 8679–8689.
24. Sun L, Hui AM, Su Q, Vortmeyer A, Kotliarov Y, Pastorino S *et al*. Neuronal and glioma-derived stem cell factor induces angiogenesis within the brain. *Cancer Cell* 2006; **9**: 287–300.
25. Gaspar C, Cardoso J, Franken P, Molenaar L, Morreau H, Moslein G *et al*. Cross-species comparison of human and mouse intestinal polyps reveals conserved mechanisms in adenomatous polyposis coli (APC)-driven tumorigenesis. *Am J Pathol* 2008; **172**: 1363–1380.
26. Hao Y, Triadafilopoulos G, Sahbaie P, Young HS, Omary MB, Lowe AW. Gene expression profiling reveals stromal genes expressed in common between Barrett's esophagus and adenocarcinoma. *Gastroenterology* 2006; **131**: 925–933.
27. Chen X, Leung SY, Yuen ST, Chu KM, Ji J, Li R *et al*. Variation in gene expression patterns in human gastric cancers. *Mol Biol Cell* 2003; **14**: 3208–3215.
28. Deng CX. BRCA1: cell cycle checkpoint, genetic instability, DNA damage response and cancer evolution. *Nucleic Acids Res* 2006; **34**: 1416–1426.
29. Yang ES, Xia F. BRCA1 16 years later: DNA damage-induced BRCA1 shuttling. *FEBS J* 2010; **277**: 3079–3085.
30. Luo Q, Lai Y, Liu S, Wu M, Liu Y, Zhang Z. Deregulated expression of DNA polymerase beta is involved in the progression of genomic instability. *Environ Mol Mutagen* 2012; **53**: 325–333.
31. Ku NO, Omary MB. A disease- and phosphorylation-related nonmechanical function for keratin 8. *J Cell Biol* 2006; **174**: 115–125.
32. Kim S, Coulombe PA. Intermediate filament scaffolds fulfill mechanical, organizational, and signaling functions in the cytoplasm. *Genes Dev* 2007; **21**: 1581–1597.
33. Sahlgren CM, Pallari HM, He T, Chou YH, Goldman RD, Eriksson JE. A nestin scaffold links Cdk5/p35 signaling to oxidant-induced cell death. *EMBO J* 2006; **25**: 4808–4819.
34. Turner NC, Lord CJ, Iorns E, Brough R, Swift S, Elliott R *et al*. A synthetic lethal siRNA screen identifying genes mediating sensitivity to a PARP inhibitor. *EMBO J* 2008; **27**: 1368–1377.
35. Tian B, Yang Q, Mao Z. Phosphorylation of ATM by Cdk5 mediates DNA damage signalling and regulates neuronal death. *Nat Cell Biol* 2009; **11**: 211–218.
36. Huang E, Qu D, Zhang Y, Venderova K, Haque ME, Rousseaux MW *et al*. The role of Cdk5-mediated apurinic/aprimidinic endonuclease 1 phosphorylation in neuronal death. *Nat Cell Biol* 2010; **12**: 563–571.
37. Bolin C, Boudra MT, Fernet M, Vaslin L, Pennaneach V, Zaremba T *et al*. The impact of cyclin-dependent kinase 5 depletion on poly(ADP-ribose) polymerase activity and responses to radiation. *Cell Mol Life Sci* 2011; **69**: 951–962.
38. Krupkova O Jr., Loja T, Redova M, Neradil J, Zitterbart K, Sterba J *et al*. Analysis of nuclear nestin localization in cell lines derived from neurogenic tumors. *Tumour Biol* 2011; **32**: 631–639.
39. Veselska R, Kuglik P, Cejpek P, Svachova H, Neradil J, Loja T *et al*. Nestin expression in the cell lines derived from glioblastoma multiforme. *BMC Cancer* 2006; **6**: 32.
40. Loja T, Chlapek P, Kuglik P, Pesakova M, Oltova A, Cejpek P *et al*. Characterization of a GM7 glioblastoma cell line showing CD133 positivity and both cytoplasmic and nuclear localization of nestin. *Oncol Rep* 2009; **21**: 119–127.
41. Yang XH, Wu QL, Yu XB, Xu CX, Ma BF, Zhang XM *et al*. Nestin expression in different tumours and its relevance to malignant grade. *J Clin Pathol* 2008; **61**: 467–473.
42. Chen Z, Wang T, Luo H, Lai Y, Yang X, Li F *et al*. Expression of nestin in lymph node metastasis and lymphangiogenesis in non-small cell lung cancer patients. *Hum Pathol* 2010; **41**: 737–744.
43. Hendrix MJ. Intermediate filaments. *Cancer Metast Rev* 1996; **15**: 413–416.
44. Hartig R, Shoeman RL, Janetzko A, Tolstonog G, Traub P. DNA-mediated transport of the intermediate filament protein vimentin into the nucleus of cultured cells. *J Cell Sci* 1998; **111**(Pt 24): 3573–3584.
45. Wang X, Tolstonog G, Shoeman RL, Traub P. Selective binding of specific mouse genomic DNA fragments by mouse vimentin filaments *in vitro*. *DNA Cell Biol* 1996; **15**: 209–225.
46. Spencer VA, Coutts AS, Samuel SK, Murphy LC, Davie JR. Estrogen regulates the association of intermediate filament proteins with nuclear DNA in human breast cancer cells. *J Biol Chem* 1998; **273**: 29093–29097.
47. Du ZM, Hu CF, Shao Q, Huang MY, Kou CW, Zhu XF *et al*. Upregulation of caveolin-1 and CD147 expression in nasopharyngeal carcinoma enhanced tumor cell migration and correlated with poor prognosis of the patients. *Int J Cancer* 2009; **125**: 1832–1841.
48. Zhong D, Xiong L, Liu T, Liu X, Liu X, Chen J *et al*. The glycolytic inhibitor 2-deoxyglucose activates multiple prosurvival pathways through IGF1R. *J Biol Chem* 2009; **284**: 23225–23233.



Cell Death and Disease is an open-access journal published by Nature Publishing Group. **Cell Death and Disease** is an open-access journal published by Nature Publishing Group. This work is licensed under a Creative Commons Attribution-NonCommercial-NoDerivs 3.0 Unported License. The images or other third party material in this article are included in the article's Creative Commons license, unless indicated otherwise in the credit line; if the material is not included under the Creative Commons license, users will need to obtain permission from the license holder to reproduce the material. To view a copy of this license, visit <http://creativecommons.org/licenses/by-nc-nd/3.0/>

Supplementary Information accompanies this paper on Cell Death and Disease website (<http://www.nature.com/cddis>)